Energy Advances

ROYAL SOCIETY OF CHEMISTRY

PAPER

View Article Online
View Journal | View Issue

Cite this: *Energy Adv.*, 2024, 3, 2587

Electrochemical and spectroscopic characterisation of organic molecules with high positive redox potentials for energy storage in aqueous flow cells†

Christopher G. Cannon,[a] Peter A. A. Klusener,[b] Nigel P. Brandon[c] and Anthony R. J. Kucernak *[a]

Received 8th June 2024,
Accepted 27th August 2024

DOI: 10.1039/d4ya00366g

rsc.li/energy-advances

We show that a number of ubiquitous organic molecules used as redox mediators and chemically sensing species can be used as positive couples in electrochemical energy storage. Air and acid stable organic molecules were tested in aqueous acid electrolytes and employed as the positive electrolyte in H_2–organic electrochemical cells. The dissolved organic species were characterised *in-operando* using UV-vis spectroscopy. *N,N,N′,N′*-tetramethylbenzidine was found to be a stable and reversible redox organic molecule, with a 2 e^- molecule^{-1} capacity and a 0.83 V cell potential. *N*-Oxyl species were also tested in purely aqueous acidic flow battery electrolytes. A H_2–violuric acid cell produced a reversible potential of 1.16 V and demonstrated promising redox flow cell cycling performance.

1. Introduction

Abundantly available materials that possess multiple oxidation states with long-term stability are greatly sought after to allow for more economically feasible large-scale energy storage devices. Hydrogen is an abundant and proven electrochemical energy storage (EES) medium but pairing it with molecular oxygen on the positive electrode, as in low-temperature H_2–O_2 polymer electrolyte membrane fuel cells (PEMFCs) and electrolysers (PEMELs), creates many issues. These are mainly related to the material requirements for platinum group metal catalysts, and the relatively poor round-trip efficiency caused by the large overpotentials needed to drive the water/oxygen reactions at high rates. Flow batteries (FBs) can avoid both of these specific issues. The most developed FB cell chemistry to date uses vanadium-based electrolytes, but vanadium resources are also a pressing limitation for this design.

The H_2–X design illustrated in Fig. 1 has all the advantages of the redox flow battery, with three further critical advantages being (i) it can use abundant energy storage media, consisting of H_2 and an aqueous electrolyte with a molecular organic redox couple, (ii) the bulk concentration overpotential affects only one side of the cell and (iii) liquid crossover to the H_2-side can be recovered with no long-term capacity loss. The names flow battery (FB) and rechargeable fuel cell (RFC) could be used interchangeably, although the latter would be more correct if the H_2-side is not a closed loop. Nanoparticulate Pt catalysts facilitate hydrogen evolution and oxidation reactions on the negative electrode but, unlike PEMFCs/PEMELs, the positive electrode reaction requires only high surface area graphitic carbon. In this design, "X" is a FB electrolyte that is pumped through the cells. In the FB literature, the positive electrolyte is commonly called either the catholyte or posolyte. Crossover,

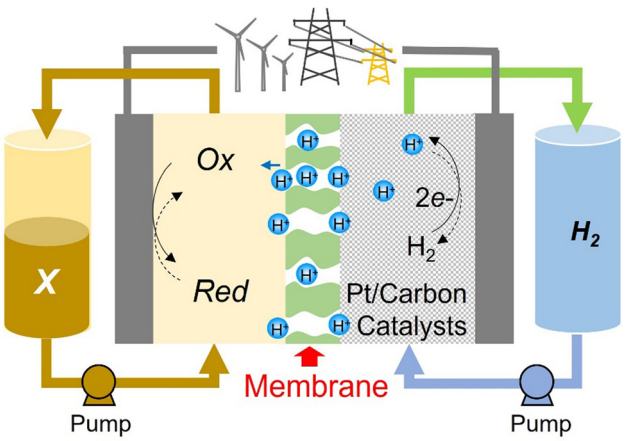

Fig. 1 Illustration of the H_2–X rechargeable fuel cell.

[a] Department of Chemistry Imperial College London MSRH, White City, London W12 0BZ, UK. E-mail: anthony@imperial.ac.uk
[b] Shell Global Solutions International B.V. Energy Transition Campus Amsterdam, Grasweg 31, 1031 HW Amsterdam, The Netherlands
[c] Department of Earth Science and Engineering Imperial College London South Kensington, London SW7 2AZ, UK

† Electronic supplementary information (ESI) available. See DOI: https://doi.org/10.1039/d4ya00366g

efficiency and the long-term stability of organic-based electrolytes are often cited as limitations, but the benefits of decoupling the energy storage capacity from materials of limited supply are well-documented.[1–3] We have therefore investigated the potentiality of various small organic molecules dissolved in purely aqueous acidic media, in conjunction with the H_2/H^+ counter-reaction, as practical H_2–X chemistries.

In this work we are focusing on low-pH electrolytes, as they operate well in conjunction with the H_2/H^+ counter-reaction. Furthermore, acidic electrolytes provide a less nucleophilic environment, in which the high oxidation state species is less likely to undergo degradation than in a high pH electrolyte. To be effective in this RFC design, the organic species acting as X must have at least two oxidation states that are chemically stable. All redox states of X must also be highly soluble and diffusive, with facile electron-transfer kinetics and a potential approaching 1.6 V *vs.* RHE in the best-case scenario. These are the general properties desired in positive flow battery electrolytes. The safety, scale and cost at which it can be produced must also be considered. Therefore, in this work we assess organic compounds that are already ubiquitous and commercially available, that they may possess the aforementioned properties to some degree. We have studied five organic redox molecules as possible X species, namely 2,2′-azinobis(3-ethylbenzothiazoline-6-sulfonate) (ABTS), chlorpromazine (CPZ), *N,N,N′,N′*-tetramethylbenzidine (TMB), *N*-hydroxyphthalimide (NHPI) and violuric acid (VIO).

ABTS is considered a safe and commonly used agent to study many reactions *via* the quantification of free radical species, and as an antioxidant assay. It is known to produce a persistent radical with a high extinction coefficient at 415 nm.[4,5] This makes it an interesting species to consider as a positive FB electrolyte. CPZ is a medicinally valuable phenothiazine, which are a class of mass-manufactured chemicals with applications such as dyes and medicines.[6] Other notable examples are promethazine, thioridazine, and methylene blue. TMB – not to be confused with 3,3,5′,5′-tetramethylbenzidine – can be synthesised *via* a straightforward one-step process of electrochemical dehydrogenative cross-coupling (effectively electro-dimerization) of *N,N*-dimethylaniline, a stock chemical in many industrial syntheses.[7,8] TMB has been investigated for many decades as a model compound for studying photochemical electron transfer processes.[9,10]

N-Oxyl radical-forming species are widely used as redox mediators and radical markers and are very commonly used in aqueous FBs already. At present, derivatives of (2,2,6,6-tetramethylpiperidin-1-yl)oxyl (TEMPO) are the most studied *N*-oxyl-based electrolytes. TEMPO is a persistent radical that readily forms a $TEMPO^+$ cation upon chemical or electrochemical oxidation, ordinarily between 0.7–1.0 V *vs.* SHE depending on the functionalisation.[11,12] However, TEMPO-based FB electrolytes are only applicable to neutral pH systems as they undergo an electrochemically irreversible disproportionation reaction in the presence of acid.[13] Other *N*-oxyl species which have only been tangentially studied for energy storage applications include NHPI, VIO, and 1-hydroxybenzotriazole (HBT). Unlike TEMPO however, the redox mechanisms of NHPI, VIO and HBT are thought to form *N*-oxyl radical species upon a proton-coupled oxidation of the *N*-hydroxyl form. The significance of these *N*-oxyl species (NHPI and VIO) is that they also both allow H_2–X cell voltages in excess of 1.0 V - and therefore higher specific energy densities than vanadium(IV/V) at an equal concentration. Tian *et al.* studied NHPI in a semi-aqueous acidic FB; an electrolyte formulated of NHPI dissolved in a mixture of acetonitrile and aqueous 1 M H_2SO_4 was cycled with a quinone molecule on the negative side in a FB cell demonstrating partial reversibility.[14] In the work described below, a fully aqueous NHPI electrolyte produced a high cell potential of 1.34 V, yet the high degradation rate prevented any reversibility in a full H_2–organic cell. VIO, which conversely performed well, has a related structure to NHPI, with carbonyl groups adjacent to an oxime group.

These redox-active organic molecules may be applicable to many electrochemical energy storage (EES) systems due to their notably high redox potentials and fast redox kinetics. In the

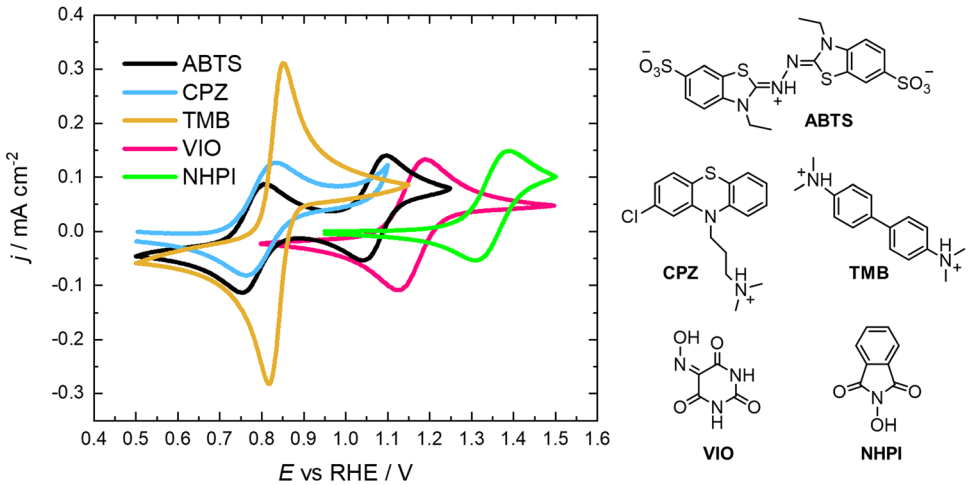

Fig. 2 Cyclic voltammograms of 2,2′-azinobis(3-ethylbenzothiazoline-6-sulfonate) (ABTS), chlorpromazine (CPZ), *N,N,N′,N′*-tetramethylbenzidine (TMB), *N*-hydroxyphthalimide (NHPI) and violuric acid (VIO); 1 mM analyte/1 M H_2SO_4 or 1 M $HClO_4$ (ABTS) and a scan rate of 50 mV s^{-1}.

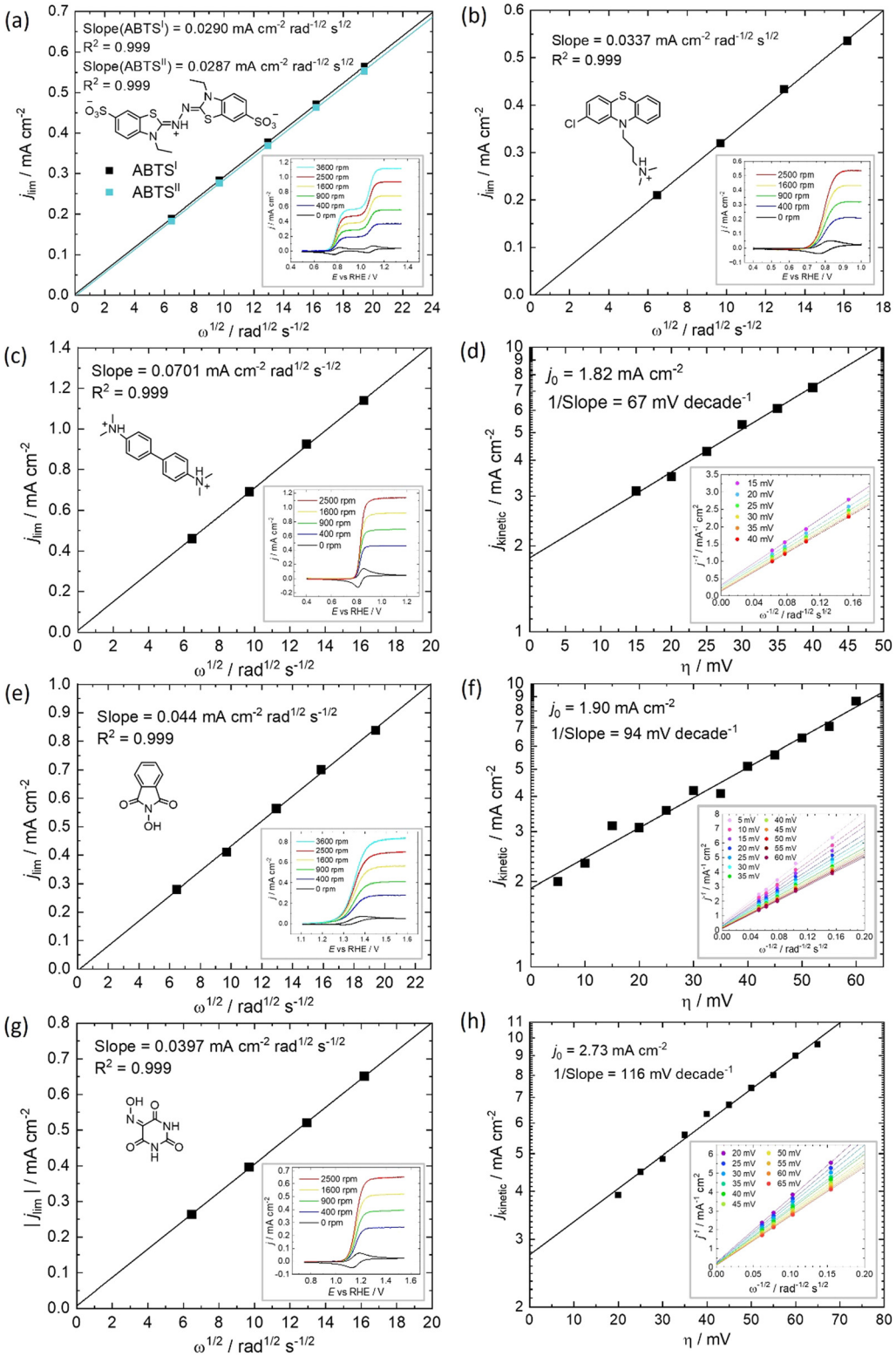

Fig. 3 Determination of diffusivity coefficient and electrokinetic parameters of 2,2′-azinobis(3-ethylbenzothiazoline-6-sulfonate) (ABTS), chlorpromazine (CPZ), *N*,*N*,*N*′,*N*′-tetramethylbenzidine (TMB), *N*-hydroxyphthalimide (NHPI) and violuric acid (VIO). Levich plot of the limiting current (i_{lim}) from iR-free and background-corrected RDE voltammetry profiles with 10 mV s^{-1} scan rate of (a) 1 mM ABTS measured at 0.907 V *vs*. RHE and the normalised limiting current ($i_{0.907V} - i_{1.247V}$) of the second-step (ABTS^{II}) in 1 M $HClO_4$, and 1 mM (b) CPZ, (c) TMB, (e) NHPI and (g) VIO in 1 M H_2SO_4 solutions. Tafel plot of the estimated linear region of the absolute kinetic current density *vs*. overpotential, from the Koutechy–Levich analysis of (e) TMB (f) NHPI and (h) VIO in 1 M H_2SO_4.

H_2–X system specifically, this work presents new organic electrolyte chemistries and the highest cell voltages achieved to date for a H_2–organic RFC, and may lead to improvements upon previous work in the energy density and overall round-trip efficiency of the H_2–X RFC.[15,16]

2. Results and discussion

2.1 Electrochemical characterisation

All of the molecules studied showed electrochemical redox activity with good reversibility. The redox potential (E^0) for each of these positive electrolyte species was measured from the centre of the cyclic voltammogram (CV) peaks shown in Fig. 2. All CVs are plotted on the RHE scale, which corresponds to the theoretical cell voltage of each H_2–X chemistry. Also shown in Fig. 2 is each structure of the reduced form of each of the species, as interpreted from inspection of the UV-vis spectra alongside existing literature (see Section 2.2).

The diffusivity coefficient (D) and the electron transfer rate constant (k_e) were obtained from rotating-disk electrode (RDE) experiments, presented in Fig. 3, and the electrochemical parameters are presented in Table 1. The two heterocyclic amines (ABTS and CPZ) both undergo extremely facile electron-transfers. For both oxidation steps of ABTS and the single e^- oxidation of CPZ, the reorganizational energy incurred is so inconsequential that kinetically limited currents were indetectable by the RDE method (see ESI,† Fig. S1). However, the diffusivity of ABTS is relatively sluggish, as D can be negatively affected by localised charges and a large molecular mass. Perchloric acid was used as the supporting electrolyte for ABTS because the product(s) of ABTS oxidation were insoluble in 1 M H_2SO_4. The solubility appeared to improve in 6 M H_2SO_4 and this formulation could be tested in a full cell (see Section 2.2), but the electrolyte formed a precipitate slowly over time. The *N*-oxyl couples (NHPI and VIO) were the lightest molecules tested (163.13 and 157.08 g mol^{-1} respectively) and have the highest diffusion coefficients. On the other hand, compared to the amine-centred redox couples (ABTS, CPZ and TMB) the electron-transfer kinetics of NHPI and VIO were found to be at least a factor of two slower, yet they were still an order of magnitude faster than many (if not all) high potential bicarbonyl- and quinone-based organic FB electrolytes.[17–19]

Table 1 displays the kinetic rate constant and the mass transfer rate constant, which allow for the evaluation of the theoretical "Intrinsic power" of any redox couple X. A hypothetical mass transfer rate constant k_m is derived from the following relationship, using the experimental $k_{m,(Fe^{2+}/Fe^{3+})}$ of 1.4×10^{-3} cm s^{-1} for the flow of iron chloride in an RFB felt at a superficial velocity of 1 cm s^{-1}.[24] The notional mass-transfer coefficient $k_{m,X}$ of any positive redox couple X was derived as shown in eqn (1), in which the diffusion coefficients of Fe^{2+}/Fe^{3+} (mean value) and of X are represented by $D_{Fe^{2+}/Fe^{3+}}$ and D_X, respectively.

$$k_{m,X} = \frac{k_{m,(Fe^{2+}/Fe^{3+})}}{\left(D_{Fe^{2+}/Fe^{3+}}\right)^{2/3}} \times (D_X)^{2/3} \quad (1)$$

For a fixed overpotential (when $j = j_0$ and $\alpha = 0.5$), the *iR*-free current consists of two terms, as shown in eqn (2) below, where j_X is the notional current density of any positive redox couple X, n is the stoichiometric number of electrons transferred, F is the Faraday constant, $k_{e,X}$ is the standard kinetic constant of X and c^* is the bulk concentration of X at 100% state-of-charge.[25]

$$\frac{1}{j_X} = \frac{1}{nFk_{e,X}c^*} + \frac{1}{nFk_{m,X}c^*} \quad (2)$$

In the case that the kinetics are too facile to be measured by the RDE method, we assume $1/k_{e,X} = 0$. The influences of both rate constants can therefore be consolidated into a composite rate constant ($k_{comp,X}$) as so

$$\frac{1}{k_{comp,X}} = \frac{1}{k_{e,X}} + \frac{1}{k_{m,X}} \quad (3)$$

The term k_{comp} is therefore a single rate constant that incorporates both k_e and D. The other key metric of a FB electrolyte is the specific energy density (E_V), which in the H_2–X system is the product of the potential (E^0 *vs.* RHE) and the specific capacity (C/A h L^{-1}). Plotted against one another, we can find the theoretical Joules per second (or Power) imparted from the positive electrolyte. This intrinsic power ($P_{intrinsic}$) is defined in eqn (4).

$$P_{intirinsic,X}\ (\times 3.6\ \text{W cm}^{-2}) = k_{comp,X}\ (\text{cm s}^{-1}) \cdot E_V\ (\text{W h L}^{-1}) \quad (4)$$

This is a useful comparator as we can extrapolate the relative merits and shortcomings of new FB electrolyte candidates from experimental data collected at very low concentrations. To do this, we have normalised the concentrations to 1 mol L^{-1}, which is equivalent to 26.8 A h L^{-1} per e^-. The end results

Table 1 Measured electrokinetic and transport parameters for 2,2′-azinobis(3-ethylbenzothiazoline-6-sulfonate) (ABTS), chlorpromazine (CPZ), *N*,*N*,*N*′,*N*′-tetramethylbenzidine (TMB), *N*-hydroxyphthalimide (NHPI) and violuric acid (VIO), assuming $\nu = 9.55 \times 10^{-3}$ and 1.23×10^{-2} cm^2 s^{-1} for 1 M $HClO_4$ and 1 M H_2SO_4 respectively[20,21]

	Supporting electrolyte	E *vs.* RHE/V	No. of e^-	$D/10^{-6}$ cm^2 s^{-1}	$k_m/10^{-6}$ cm s^{-1}	$k_e/10^{-2}$ cm s^{-1}	$k_{comp.}/10^{-4}$ cm s^{-1}
ABTS^{I}	1 M $HClO_4$	0.78	1	3.3	8.86	$>10^a$	8.9
ABTS^{II}	1 M $HClO_4$	1.26	1	3.3	8.77	$>10^a$	8.8
CPZ	1 M H_2SO_4	0.80	1	4.5	10.8	$>10^a$	10.8
TMB	1 M H_2SO_4	0.83	2	4.8	11.2	0.9	10.0
NHPI	1 M H_2SO_4	1.34	1	6.7	14.1	2.0	13.1
VIO	1 M H_2SO_4	1.16	1	5.7	12.7	2.8	12.2

[a] Electrokinetics too fast to measure with RDE technique.[22,23]

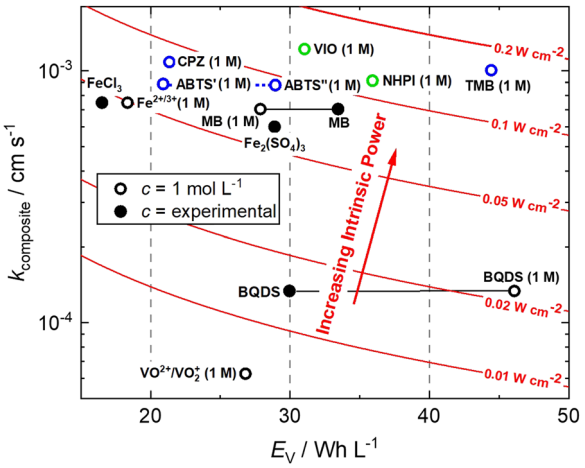

Fig. 4 Intrinsic power of organic redox couples in a hypothetical H_2–X RFC.[15,16,24,26–28] ABTS: 2,2′-azinobis(3-ethylbenzothiazoline-6-sulfonate); BQDS: 2-dihydrobenzoquinone-3,5-disulfonic acid; CPZ: chlorpromazine; MB: methylene blue; NHPI: *N*-hydroxyphthalimide; TMB: *N*,*N*,*N*′,*N*′-tetramethylbenzidine; VIO: violuric acid.

are plotted in Fig. 4. ABTS, CPZ and TMB are highlighted in blue and the *N*-oxyl couples NHPI and VIO are shown in green.

We have previously studied 1,2-dihydrobenzoquinone-3,5-disulfonic acid (BQDS) and methylene blue (MB) in the H_2–X RFC, which achieved electrolyte concentrations of 0.65 M and 1.2 M respectively.[15,16] Tucker *et al.* investigated $FeCl_3$ and $Fe_2(SO_4)_3$ salts in a H_2–Fe RFC, tested at 0.9 M and 0.7 M respectively.[29] These two RFB chemistries are also presented in Fig. 4, at their theoretical energy densities. From this information we can see that the rate constants of organic molecules are either comparable to or exceeding that of typically used metallic FB electrolyte ions of Fe and V. At concentrations of 1 mol L^{-1}, the positive electrolyte capacities are all in excess of 20 W h L^{-1}, with TMB achieving a theoretical capacity of 44.5 W h L^{-1}. TMB also has the highest $P_{intrinsic}$ value, followed closely by VIO, which although having a lower theoretical capacity makes up for this deficit by having a higher composite rate constant.

2.2. Evaluation of H_2–organic cycling in a full cell

All of the redox couples were tested in a flow cell at a concentration of 5 mM in an appropriate supporting electrolyte, using a constant charge–discharge current density of 5 mA cm^{-2}, with a 300 s open-circuit intermission between applied charge and discharge currents. The organic couples were the capacity limiting component of the cells. Galvanostatic cycling indicates the fade of the capacity-limiting electrolyte, yet it is important to note that the state-of-charge (SoC) achieved *via* this method can be subject to variations in the cell resistance and may not be an accurate quantification of capacity fade. To monitor the fade of relatively stable electrolytes, potentiostatic holds to complete conversion may be

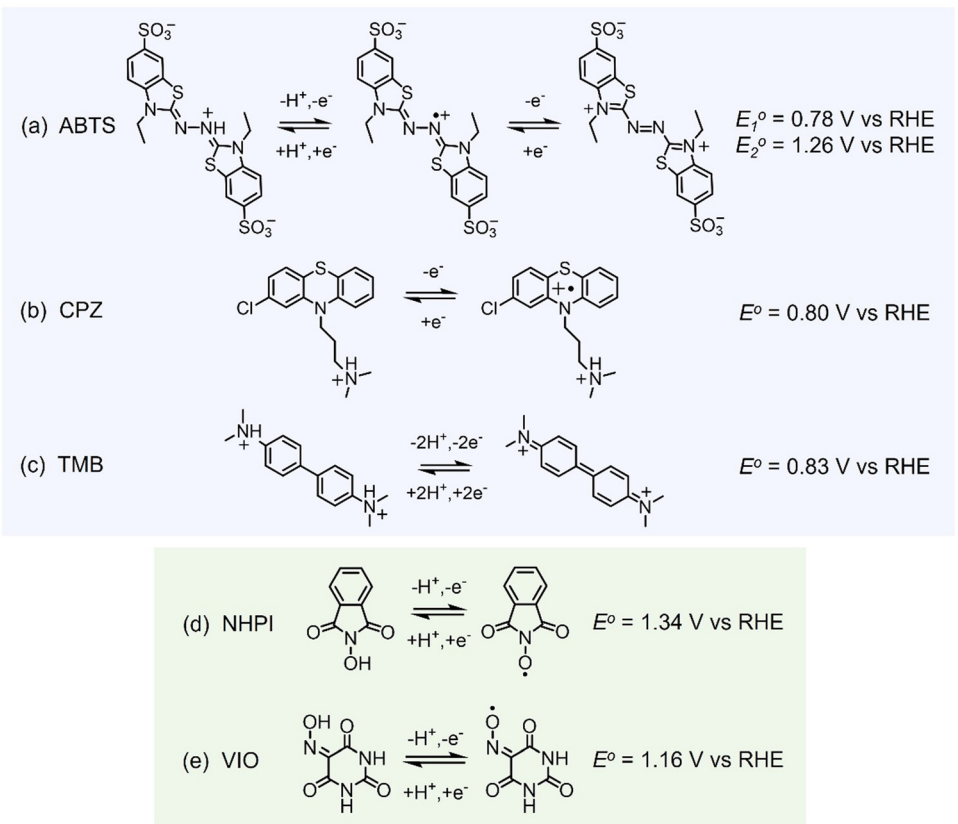

Fig. 5 Determined redox reactions and potentials for (a) 2,2′-azinobis(3-ethylbenzothiazoline-6-sulfonate) (ABTS) in 1 M $HClO_4$, and (b) chlorpromazine (CPZ), (c) *N*,*N*,*N*′,*N*′-tetramethylbenzidine (TMB),(d) *N*-hydroxyphthalimide (NHPI) and (e) violuric acid (VIO), in 1 M H_2SO_4.

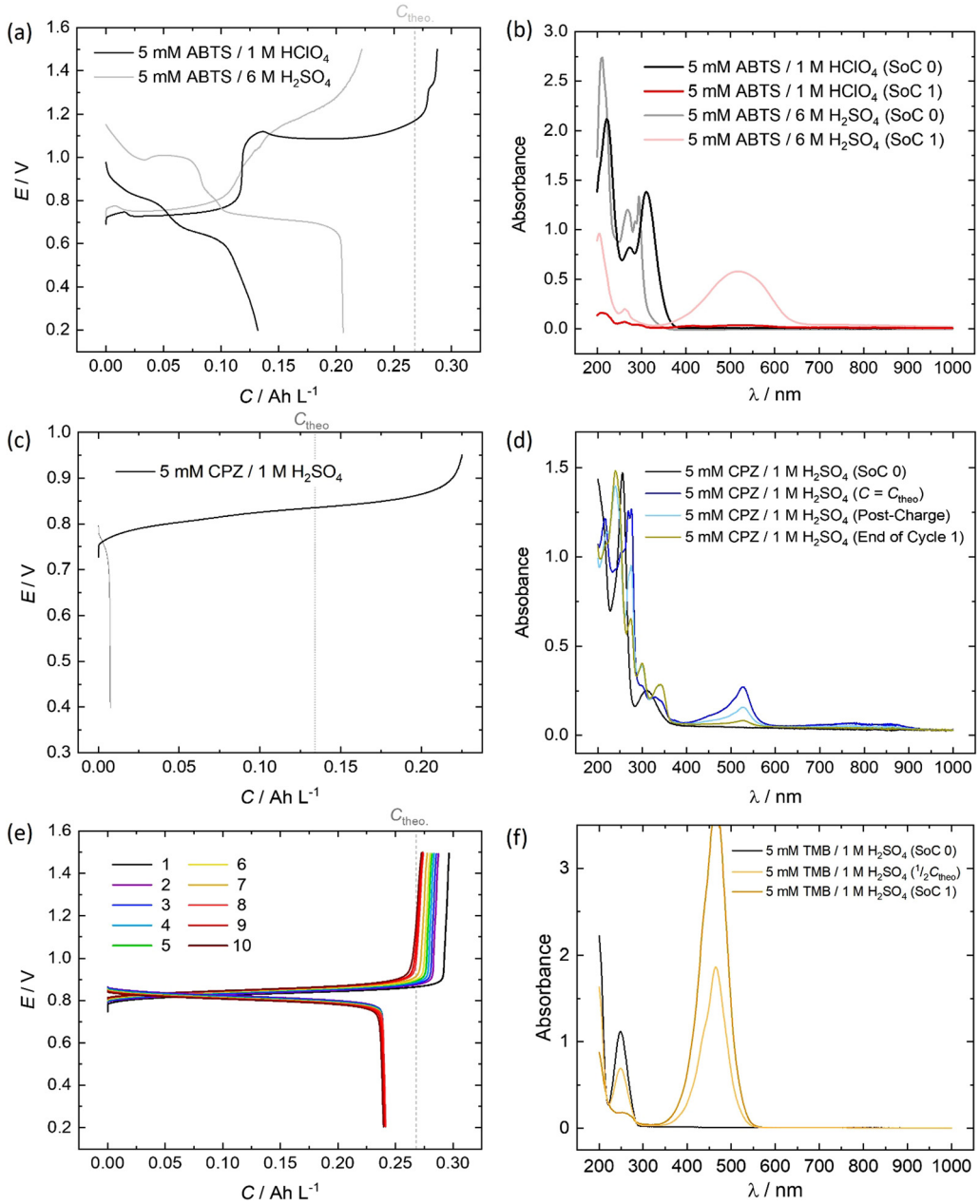

Fig. 6 RFC test of 5 mM organic in 100 mL electrolyte cycled galvanostatically at 5 mA cm^{-2} and *in-operando* recorded UV-vis spectra at key points during the initial cycle of (a) and (b) ABTS, (c) and (d) CPZ and (e) and (f) TMB.

required. The UV-vis absorption spectrum (200–1000 nm) of the electrolyte was monitored throughout the initial cycle using a separate pumped electrolyte circuit (see ESI,† Fig. S2). From this information the initial structures in Fig. 5 of the organic species participating in the redox reactions were inferred.

In neutral solution, ABTS dissolves as $ABTS^{2-}$. The oxidation of $ABTS^{2-}$ (colourless) to the radical $ABTS^{\bullet-}$ is a useful kinetic probe due to the fast electron transfer in aqueous solutions.[30] Scott *et al.* determined the pK_a of $ABTS^{2-}$ to form $HABTS^-$ to be 2.08, and the spectroscopic analysis (Fig. 6b) of 5 mM ABTS in 1 M $HClO_4$ at the 0% state-of-charge (SoC 0) was consistent with $HABTS^-$.[30] $ABTS^{\bullet-}$ is a metastable radical, aqueous samples of which are often prepared the day before use, as they can be stored overnight.[31] It is possible that the comproportionation reaction in eqn (R1), between unprotonated $ABTS^{2-}$ and doubly oxidised state $ABTS^0$, complicates further oxidation.[4]

$$ABTS^0 + ABTS^{2-} \rightarrow 2\ ABTS^{\bullet-} \quad (R1)$$

In solutions of 1 M H_2SO_4, 1 mM ABTS requires a high scan rate (or a sub-millimolar concentration) to see a cathodic peak for the reduction of $ABTS^0$, whereas in $HClO_4$ both redox processes are reversible.[4,30] The cell potential *vs.* capacity profile of 5 mM ABTS/1 M $HClO_4$ in Fig. 6a indicates a possible self-discharge of the doubly oxidised state, as the first half of

the charge process reaches a mass-transport overpotential before the $\frac{1}{2}C_{theo}$ point of 0.134 A h L^{-1}. During cycling, spectra appeared that were consistent with radical formation. However, the radical spectrum fluctuated at low levels with maximum intensities shortly after the charge starts and near $\frac{1}{2}C_{theo}$ and did not linearly accumulate in the manner expected as though it were the product of bulk oxidation (see ESI,† Fig. S3).

When using 6 M H_2SO_4 as the supporting electrolyte, the H_2–ABTS cell did not overshoot the theoretical maximum amount of charge transferred for 2 e^- oxidation per molecule. In the initial (SoC 0) spectrum, the characteristic $HABTS^-$ peak was red-shifted to 294 nm with a shoulder at 285 nm. The capacity attained at 5 mA cm^{-2} was lower than in 1 M $HClO_4$, but the whole cycle was completed in a similar timeframe (56 min *vs.* 55 min) with a 92.7% coulombic efficiency, compared to 45.8% for 5 mM ABTS in 1 M $HClO_4$. The spectrum recorded at the maximum state-of-charge achieved (SoC 1), was characteristic of $ABTS^0$, which notably was not apparent when 1 M $HClO_4$ was used.[32] It is important to note that the intensity of this peak (λ_{max} = 516 nm) decayed by approximately $\frac{1}{3}$rd in the 5-minute open-circuit time period before the discharge process began. As was also mentioned in the previous section, after standing, the 5 mM ABTS/6 M H_2SO_4 sample accumulated dark blue precipitate (ESI,† Fig. S4).

The oxidation and reduction of CPZ in 1 M H_2SO_4 is shown in Fig. 2 by a reversible cyclic voltammogram, which has a slight hysteresis possibly due to a layer of by-products that formed on the glassy carbon electrode surface following the oxidation of CPZ. The literature pK_a of CPZ is 9.2–9.3, and so under the acidic conditions of the H_2–X RFC the amine side-chain was considered to be protonated.[33,34] The redox reaction of CPZ to form $CPZ^{\bullet+}$ at ~0.8 V *vs.* SHE is well-documented.[35] It has also been shown to have a proton independent potential between pH 1.8–7.4, but that the temporal stability of the radical improves at lower pH.[35] A second oxidation with an onset ~1 V *vs.* RHE in 1 M H_2SO_4 showed no cathodic current. CPZ was therefore cycled in the cell with a potentiometric cut-off of only 0.95 V, to prevent the second electrochemical oxidation from occurring. The cell potential *versus* capacity profile is shown in Fig. 6c. Upon charging, the *in-operando* UV-vis spectra revealed the presence of a new species with a peak at λ_{max} = 530 nm (Fig. 6d), which was characteristic of the vibrant red $CPZ^{\bullet+}$ radical.[36–38] For the full set of spectra obtained during the charging step see ESI,† Fig. S5. Despite the low cut-off cell voltage, the CPZ charging process smoothly surpassed the theoretical 1 e^- per molecule capacity of 0.134 A h L^{-1} (C_{theo}). The absorption peak at λ_{max} = 530 nm (assigned to $CPZ^{\bullet+}$) decreased slowly after C_{theo}, and then decreased rapidly during the brief discharge process. The cell potential was high as the discharge commenced, indicating facile reversibility, however within a very short time the cell appeared to reach a reactant mass transport overpotential as a result of a low starting concentration of $CPZ^{\bullet+}$. One explanation for the poor cyclability observed is the disproportionation of the radical in acidic solution as described in eqn (R2), which has also been put forward by Zhang *et al.*[35]

$$2\ CPZ^{\bullet+} \rightarrow CPZ + CPZ^{2+} \quad (R2)$$

Emergent peaks at 240, 300 and 340 nm develop throughout the charging process, and are seen in the light blue spectrum in Fig. 6d, recorded immediately after the galvanostatic charge process. These three peaks are consistent with literature analyses of chlorpromazine sulfoxide (CPZO) absorption, and their intensity was unaffected even after the discharge process, shown by the green spectrum.[39] CPZ^{2+} is thought to be reactive with water and quickly hydrolyses to form the sulfoxide, as shown in eqn (R3).[35,40,41]

$$CPZ^{2+} + H_2O \rightarrow CPZO + 2\ H^+ \quad (R3)$$

Therefore, it was shown that CPZ forms a significant amount of an electrochemically irreversible by-product before either a mass transport limit or the 0.95 V potentiometric limit was reached. This appeared to be due in part to a disproportionation reaction of $CPZ^{\bullet+}$, and only residual $CPZ^{\bullet+}$ allowed for a short-lived discharge current.

As shown in Fig. 6e, a H_2–TMB cell could be cycled repeatedly and with a 99.8% discharge capacity retention over the course of 10 complete cycles (fade rate ~0.2% day^{-1}). The initial spectra of uncharged 5 mM TMB in 1 M H_2SO_4 electrolyte (Fig. 6f) showed a single absorption peak at λ_{max} = 249 nm, which was consistent with the literature reports of 250 nm for the di-protonated $TMBH_2^{2+}$ species.[42–44] The behaviour and decay pathways of the oxidised states of TMB are dependent upon the degree of protonation.[42] The disproportionation of the singly oxidised radical ($TMB^{\bullet+}$) in acidic solution, as written in eqn (R4), with an equilibrium considerably to the right, has been documented in prior studies.[43] The thermodynamic instability of $TMB^{\bullet+}$ is also supported by the peak separation of 29 mV in the CV of TMB in 1 M H_2SO_4 in this work (Fig. 2).

$$2\ TMB^{\bullet+} + 2\ H^+ \rightarrow TMBH_2^{2+} + TMB^{2+} \quad (R4)$$

When a 5 mA cm^{-2} charging current was applied in the H_2–TMB cell, the $TMBH_2^{2+}$ peak linearly decreased and was replaced by the characteristic spectrum of the TMB^{2+} dication, with a λ_{max} = 465 nm, showing three isosbestic points at approximately 216.5, 222 and 284 nm. No perceivable absorption that could be attributed to the $TMB^{\bullet+}$ radical was observed.[42] A self-discharge reaction was evident from the voltage profiles and the spectral transformation over time, yet this could be largely mitigated by increasing the acid strength to 6 M H_2SO_4, in which case the cell no longer over-charged and the TMB^{2+} absorption peak retained 99.5% of its 'SoC 1' intensity over 72 h, measured at 425 nm (ESI,† Fig. S6).

The initial (SoC 0) spectrum of 5 mM NHPI in Fig. 7b was consistent with previous literature characterisations.[14,45] During charging, the electrolyte turned from colourless to yellow, which is expected when the phthalimide *N*-oxyl (PINO) radical is formed. It can be assumed that the majority of PINO generated in the electrochemical cell also self-discharged to NHPI, which accounts for the 460% overcharge seen in Fig. 7a. No discharge current of the NHPI/PINO electrolyte was sustained at a current density of 5 mA cm^{-2}, and the 'Post-Charge' spectrum in Fig. 7b characterises a degradation product.

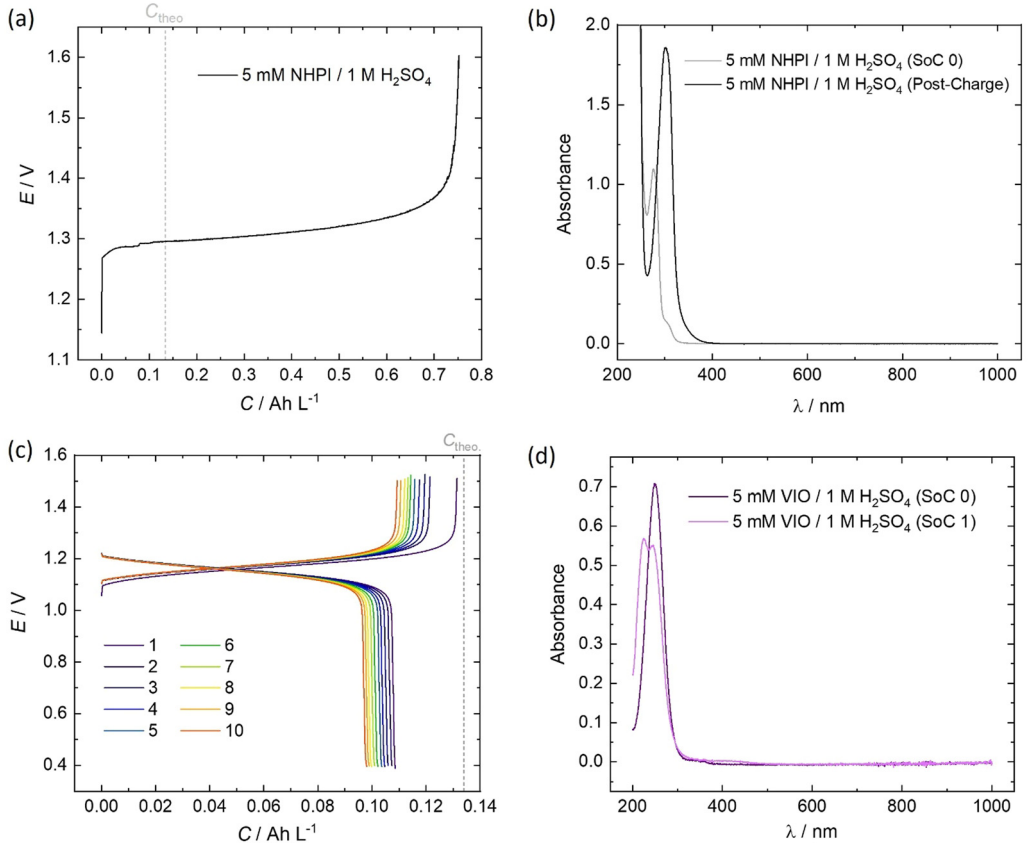

Fig. 7 RFC test of 5 mM organic in 100 mL electrolyte cycled galvanostatically at 5 mA cm^{-2} and *in-operando* recorded UV-vis spectra at key points during the initial cycle of (a) and (b) NHPI and (c) and (d) VIO.

In MeCN, VIO has a λ_{max} = 250 nm, which was also seen in Fig. 7d for the spectrum of 5 mM VIO in 1 M H_2O_4.[45] The charged state ('SoC 1') exhibited a red-shifted spectrum with an isosbestic point at 236.5 nm shared by the discharged and charged electrolyte. A lower coulombic efficiency can be reasonably expected on the first cycle, to account for the residual capacity in the depth-of-discharge attained at a fixed current density. However, as shown by the cell potential *vs.* specific capacity profiles in Fig. 7a, every charge of VIO was longer than the discharge, indicating some temporal instability. The small decrease of 9.7% in the discharge capacity over the course of 10 cycles (10.3 h) also indicates electrochemically irreversible degradation (~23% day^{-1}).

Table 2 Positive electrolyte concentration and energy density achieved

	Solvent	Conc./M	No. of e^-	E_V (*vs.* H_2)/W h L^{-1}
ABTS	1 M $HClO_4$	n.a.	2	
CPZ	1 M H_2SO_4	0.860	1	18.4
TMB	1 M H_2SO_4	0.825	2	36.7[a]
	6 M H_2SO_4	1.702		75.7
NHPI	1 M H_2SO_4	0.008	1	0.27
VIO	1 M H_2SO_4	0.033	1	1.0

[a] This will be limited by the amount of H^+ in the acidic electrolyte solution to produce H_2.

The final property to consider is the energy density that organic electrolytes can achieve. The solubility of the starting compound/organic salt in a solvent of acidic supporting electrolyte can give an idea of the suitability of each in a purely aqueous environment. Table 2 lists the maximum solubility attained in a solvent of the supporting electrolyte used in the tests in this work. Other than the molecular structure, the solubility can also be optimised by varying the ionic strength, temperature and counterion in some cases.

3. Conclusions

In recent years, a sizable collection of organic-based positive FB electrolytes have been studied.[13] However, few have the requisite characteristics in terms of a high potential, stability and other important parameters. Many of the candidates applicable to the H_2–X system are quinones or other bicarbonyl structures, yet here we have exclusively looked at alternative redox-active structural motifs to carbonyl-based couples.[46]

As well as exploring new classes of organic molecules, it is also crucial to consider the suitability of the supporting electrolyte. As we have seen here and in our previous work, the impact of modifying the composition or ionic strength can have a drastic effect on the FB electrolyte characteristics, and should not be overlooked.[15] For example, it was found that TMB^{2+}

appears to temporally decay to $TMBH_2^{2+}$ in 1 M H_2SO_4, whereas in 6 M H_2SO_4 the absorbance (and therefore inferred concentration) of TMB^{2+} showed a decay of only 0.168% per day. As was also previously mentioned, there is a pH-dependence to the stability of $CPZ^{\bullet+}$ and $ABTS^{\bullet-}$, and due to the extremely facile electrokinetics of these FB electrolyte chemistries the opportunity to improve their stability should be considered. The cell cycling performances and UV-vis spectra of H_2–ABTS cells were also thoroughly inconsistent between electrolytes with supporting solutions of 6 M H_2SO_4 and 1 M H_2SO_4. Therefore, the effects of acid composition and pH on the stability and reversibility of promising organic electrolytes such as these provide scope for future investigation.

To summarise, we have demonstrated that several high potential FB electrolytes comprising of commercially prominent organic molecules can be used for energy storage. Three of the organic candidates investigated (ABTS, NHPI and VIO) undergo highly reversible redox reactions at potentials of >1.0 V *vs.* RHE. This corresponds to a higher cell potential than the H_2–V RFC system. The H_2–VIO cell in particular was shown to cycle with promising reversibility, and with a cell potential only 0.1 V lower than the V–V symmetrical FB system. Although it has only a 1 e^- mol^{-1} capacity, the VIO redox couple has shown promising aqueous stability, and the high redox potential proves that *N*-oxyl compounds can be suitable candidates for acidic FB electrolyte systems. In practise, organic-based FB electrolytes may help separate the overall CAPEX (per kWh) of EES from the value of non-abundant metals.

4. Experimental section

Electrochemical characterisation data was obtained using a 5 mm polished glassy carbon disk as the working electrode in a rotor (Pine instruments), a graphite rod counter electrode, and a saturated calomel electrode (SCE) reference or an in-house made reversible hydrogen electrode (RHE) in a 3-compartment cell. All results were recorded on a Autolab PGSTAT302N and corrected to the RHE scale. Rotating disk electrode (RDE) measurements were recorded at a scan rate of 10 mV s^{-1}. All RDE data was iR and background corrected. Cyclic voltammograms were measured at a scan rate of 50 mV s^{-1} and background corrected. Diammonium 2,2′-azinobis(3-ethylbenzothiazoline-6-sulfonate), *N*-hydroxyphthalimide and chlorpromazine hydrochloride (Sigma Aldrich), *N*,*N*,*N*′,*N*′-tetramethylbenzidine (Thermo Scientific Chemicals) and violuric acid (Alfa Aesar) were used as received. Aqueous electrolyte solutions of were prepared using 95% H_2SO_4 (Normapur, VWR) or 60% $HClO_4$ (VWR) diluted with 18.2 MΩ ultrapure water from a Sartorius system. All 2- and 3-electrode measurements were performed at room temperature.

Electrochemical flow-cell experiments were recorded using a Scribner 857 RFB test station. Galvanostatic charge–discharge cycles were performed using a 5 cm^2 cell at ±5 mA cm^{-2} to the maximum possible depth-of-discharge within custom cell voltage limits, using 100 mL electrolyte samples. 190 μm, 0.4 mg_{Pt} cm^{-2} electrode (ELE0201, Johnson Matthey Fuel Cells) was used for the H_2-side electrode, and 4.6 mm carbon felt (Sigracell) for the liquid side, which was oxygen plasma treated (Diener) immediately before use. For ABTS cell tests, Nafion 212 was pre-treated by soaking the membrane in 5% H_2O_2 for 1 h at 80 °C. This was repeated with ultrapure pure water, then 1 M H_2SO_4. For all other cell tests the phosphoric acid-doped PBI (Celtec, BASF) membrane was used as received. The gaskets (Tygaflor) ensured membrane electrode assembly was compressed by ∼20% with 4.0 N m applied torque to the 5 cm^2 flow cell (Scribner Associates). Hydrogen gas was produced from an electrolyser (60H-FUEL Hydrogen Generator, Parker) and flowed at a 100 mL min^{-1} constant rate using a H_2 mass-flow controller (El-Flow Select, Bronkhorst) and the relative humidity was set at 98–100% by flowing through a humidification column (Perma Pure MH-110-12S-2). The positive electrolyte was flowed at a constant rate of 50 mL min^{-1} and without any protection from air. *In-operando* absorption spectra were recorded on a UV-vis photospectrometer (Evolution 220, Thermo Scientific) with a flow-through cuvette of 0.01 cm path (48/Q/0.1, Starna) or a 0.2 cm cuvette (48-4/Q/2, Starna) for the NHPI cell test, with the wavelength range of 1000–200 nm and a frequency of 1 spectrum min^{-1}.

The maximum concentrations were determined from the magnitude of the absorbance, within the calibration range (Fig. S7, ESI†) of the absorbance. The peak absorbance was measured in a 1 cm path length quartz cuvette. Each compound/organic salt was added to a supporting electrolyte solution until saturation, at room temperature. The liquid phase was isolated by passing the saturated mixture through a syringe-filter (PTFE 0.2 μm, fisherbrand) and was then diluted in 1 M H_2SO_4 to obtain a peak absorption within the calibration range, where the Beer–Lambert law was applicable.

Author contributions

CC and AK conceived the MS; CC performed all the experiments under the supervision of AK, NB and PK. CC wrote the MS with additions by AK; All authors contributed to editing the MS.

Data availability

Data for this article, used in the production of the figures are available at **https://doi.org/10.5281/zenodo.13712672**.

Conflicts of interest

One of us (Kucernak) is inventor on a patent application for organic hydrogen reversible fuel cells (WO2020109807A1). CC, AK and NB are coinventors on a patent application has been filed on aspects of this work.

Acknowledgements

One of us (CC) acknowledges the support of UKRI and Shell Global Solutions International B.V. for an Industrial CASE

studentship (210104). We acknowledge the kind donation of Celtec membranes from BASF.

References

1 R. M. Darling, K. G. Gallagher, J. A. Kowalski, S. Ha and F. R. Brushett, *Energy Environ. Sci.*, 2014, **7**, 3459–3477.
2 S. Gentil, D. Reynard and H. H. Girault, *Curr. Opin. Electrochem.*, 2020, **21**, 7–13.
3 V. Singh, S. Kim, J. Kang and H. R. Byon, *Nano Res.*, 2019, **12**, 1988–2001.
4 R. Bourbonnais, D. Leech and M. G. Paice, *Biochim. Biophys. Acta, Gen. Subj.*, 1998, **1379**, 381–390.
5 B. S. Wolfenden and R. L. Willson, *J. Chem. Soc., Perkin Trans. 2*, 1982, 805–812.
6 F. López-Muñoz, C. Alamo, G. Rubio and E. Cuenca, *Prog. Neuro-Psychopharmacol. Biol. Psychiatry*, 2004, **28**, 205–208.
7 X. Liu, T.-C. Cai, D. Guo, B.-B. Wang, S. Ying, H. Wang, S. Tang, Q. Shen and Q.-W. Gui, *Tetrahedron Lett.*, 2021, **70**, 153021.
8 T. Gessner and U. Mayer, *Ullmann's Encyclopedia of Industrial Chemistry*, Wiley-VCH Verlag GmbH & Co. KGaA, 2000.
9 V. Guichard, A. Bourkba, O. Poizat and G. Buntinx, *J. Phys. Chem.*, 1989, **93**, 4429–4435.
10 Y. Hirata, M. Takimoto and N. Mataga, *Chem. Phys. Lett.*, 1983, **97**, 569–572.
11 W. Zhou, W. Liu, M. Qin, Z. Chen, J. Xu, J. Cao and J. Li, *RSC Adv.*, 2020, **10**, 21839–21844.
12 T. Janoschka, N. Martin, M. D. Hager and U. S. Schubert, *Angew. Chem., Int. Ed.*, 2016, **55**, 14427–14430.
13 C. G. Cannon, P. A. A. Klusener, N. P. Brandon and A. Kucernak, *ChemSusChem*, 2023, e202300303.
14 Y. Tian, K. H. Wu, L. Cao, W. H. Saputera, R. Amal and D. W. Wang, *Chem. Commun.*, 2019, **55**, 2154–2157.
15 C. G. Cannon, P. A. A. Klusener, L. F. Petit, T. Wong, A. Wang, Q. Song, N. P. Brandon and A. R. J. Kucernak, *ACS Appl. Energy Mater.*, 2024, **7**, 2080–2087.
16 J. Rubio-Garcia, A. Kucernak, A. Parra-Puerto, R. Liu and B. Chakrabarti, *J. Mater. Chem. A*, 2020, **8**, 3933–3941.
17 Y. Xu, Y. Wen, J. Cheng, Y. Yanga, Z. Xie and G. Cao, WNWEC 2009 - 2009 World Non-Grid-Connected Wind Power and Energy Conference, 2009, 475-478.
18 L. Hoober-Burkhardt, S. Krishnamoorthy, B. Yang, A. Murali, A. Nirmalchandar, G. K. S. Prakash and S. R. Narayanan, *J. Electrochem. Soc.*, 2017, **164**, A600–A607.
19 A. W. Lantz, S. A. Shavalier, W. Schroeder and P. G. Rasmussen, *ACS Appl. Energy Mater.*, 2019, **2**, 7893–7902.
20 L. H. Brickwedde, *J. Res. Natl. Bur. Stand.*, 1949, **42**, 309.
21 H. E. Darling, *J. Chem. Eng. Data*, 1964, **9**, 421–426.
22 A. J. Bard and L. R. Faulkner, *Electrochemical methods: fundamentals and applications*, John Wiley & Sons, Inc., Hoboken, NJ, 2nd edn, 2001.
23 H. Wang, S. Y. Sayed, E. J. Luber, B. C. Olsen, S. M. Shirurkar, S. Venkatakrishnan, U. M. Tefashe, A. K. Farquhar, E. S. Smotkin, R. L. McCreery and J. M. Buriak, *ACS Nano*, 2020, **14**, 2575–2584.
24 X. You, Q. Ye and P. Cheng, *J. Electrochem. Soc.*, 2017, **164**, E3386–E3394.
25 C. M. A. Brett and A. M. O. Brett, *Kinetics and Transport in Electrode Reactions*, Oxford University Press, 1993.
26 D. Stephenson, S. Kim, F. Chen, E. Thomsen, V. Viswanathan, W. Wang and V. Sprenkle, *J. Electrochem. Soc.*, 2012, **159**, A1993–A2000.
27 T. Yamamura, N. Watanabe, T. Yano and Y. Shiokawa, *J. Electrochem. Soc.*, 2005, **152**, A830.
28 D. C. Harris, *Quantitative Chemical Analysis*, W.H. Freeman and Company, New York, 6th edn, 2003.
29 M. C. Tucker, V. Srinivasan, P. N. Ross and A. Z. Weber, *J. Appl. Electrochem.*, 2013, **43**, 637–644.
30 S. L. Scott, W. J. Chen, A. Bakac and J. H. Espenson, *J. Phys. Chem.*, 1993, **97**, 6710–6714.
31 I. R. Ilyasov, V. L. Beloborodov, I. A. Selivanova and R. P. Terekhov, *Int. J. Mol. Sci.*, 2020, **21**, 1131.
32 L. Venkatasubramanian and P. Maruthamuthu, *Int. J. Chem. Kinet.*, 1989, **21**, 399–421.
33 T. Kitagawa, A. Mastumoto, I. Terashima and Y. Uesono, *J. Med. Chem.*, 2021, **64**, 3885–3896.
34 F. Martinez-Rojas, C. Espinosa-Bustos, G. Ramirez and F. Armijo, *Electrochim. Acta*, 2023, **443**, 141873.
35 M. Zhang, W.-Q. Bao, Y. Wang, N. Deng and J.-B. He, *J. Electroanal. Chem.*, 2014, **724**, 1–7.
36 D. Daniel and I. G. R. Gutz, *J. Pharm. Biomed. Anal.*, 2005, **37**, 281–286.
37 E. Bosch and J. K. Kochi, *J. Chem. Soc., Perkin Trans. 1*, 1995, 1057–1064.
38 K. Minakata, O. Suzuki, Y. Ishikawa, H. Seno and N. Harada, *Forensic Sci. Int.*, 1992, **52**, 199–210.
39 A. A. Fasanmade and A. F. Fell, *Analyst*, 1985, **110**, 1117–1124.
40 G. R. Buettner, A. G. Motten, R. D. Hall and C. F. Chignell, *Photochem. Photobiol.*, 1986, **44**, 5–10.
41 A. G. Motten, G. R. Buettner and C. F. Chignell, *Photochem. Photobiol.*, 1985, **42**, 9–15.
42 R. Arce and L. Kevan, *J. Chem. Soc., Faraday Trans. 1*, 1985, **81**, 1669–1676.
43 S. M. Beck and L. E. Brus, *J. Am. Chem. Soc.*, 1983, **105**, 1106–1111.
44 S. Hashimoto and J. K. Thomas, *J. Phys. Chem.*, 1984, **88**, 4044–4049.
45 M. Homocianu, G. Biliuta, A. Airinei and S. Coseri, *Optoelectron. Adv. Mater., Rapid Commun.*, 2011, **5** 567–571.
46 P. Fischer, P. Mazúr and J. Krakowiak, *Molecules*, 2022, **27**, 560.